SOME TURBULENCE CHARACTERISTICS OF CONVECTIVELY MIXED LAYERS OVER RUGGED AND HOMOGENEOUS TERRAIN †

B. P. HUYNH*

School of Mechanical Engineering, University of Technology, Sydney, NSW, Australia

C. E. COULMAN*

Université de Nice, Departement d'Astrophysique, Nice, Cedes, France

and

T. R. TURNER**

Department of Mathematics, University of New Brunswick, Fredericton, New Brunswick, Canada

(Received in final form 25 September, 1989)

Abstract. Turbulence characteristics of convectively mixed layers over rugged and homogenous terrain are presented, and their differences are sought. The data used in the study were obtained from aircraft-borne instruments. Apart from statistics related to the mixing ratio q, there does not seem to be a marked difference between the two sets of data. This lack of difference is attributed to the degree of ruggedness of the terrain and the dominant wind direction. The behaviour of some statistics related to q is attributed to the entrainment effect of the unstable layer of the moist, cool air above the mixed layer.

1. Introduction

Although the investigation of the turbulence structure in the atmospheric boundary layer over homogeneous terrain has had a long history, it is only recently that similar work over rugged terrain has been carried out (Panofsky *et al.*, 1982; Kaimal *et al.*, 1982; Druilhet *et al.*, 1983a). Considering that most terrain is rugged to some extent, the investigation of the atmospheric boundary layer over complex terrain is somewhat overdue. In this paper, we report some turbulence characteristics in boundary layers in convective conditions. The data were collected by an instrumented aircraft over both homogeneous and rugged terrain. A parallel presentation of data will be made so that any dissimilarity, or lack of it, between homogeneous and rugged terrain cases can be identified. We present our data against the background of some published results by other workers.

† This work was initiated and a large part of it was completed while all three authors were with CSIRO (Commonwealth Scientific Industrial Research Organisation), Australia.

* Formerly at: Division of Atmospheric Research, CSIRO, Epping, NSW, Australia.

** Formerly at: Division of Mathematics and Statistics, CSIRO, Lindfield, NSW, Australia.

Boundary-Layer Meteorology **51**: 229–254, 1990.

2. The Observation Program

2.1. Generalities

The observation program was carried out on board the CSIRO research aircraft, an F-27. This aircraft is fitted with a 6.5 m long nose boom, and the instruments for measuring air motion and temperatures are fitted on the front part of this boom, relatively free from the aircraft-induced effects. Table I shows further details about the instruments used.

A total of four days worth of observations are studied in this report. On two of these days (involving 32 runs), the observations were obtained over rugged terrain. On the other two days (19 runs) they were obtained over relatively homogeneous terrain. These four days are designated as C12, C13, M23 and M29 as shown in Table II. The days and times chosen for observation – usually between mid-day and early afternoon – are such that fairly steady convective conditions are ensured to be dominant. Table II shows some more details about the observation program, meteorological and ground conditions.

Each aircraft 'production' run was done at a constant altitude and in a straight line about 15 km long. Each run lasted about 3 min. The altitudes, however, varied among the runs, so that the boundary-layer mid-region of between $0.04z_i$ and $0.8z_i$, where z_i is the mixed-layer height, was covered. Spiral soundings over the centre parts of the investigated regions were carried out immediately before the first run and after the last run of the observation 'day', to determine the instantaneous values of z_i. The values of z_i at intermediate times were then interpolated from these two readings. For M29, however, due to the short time involved, only one sounding was made at the end of the series of runs, and the z_i value thus determined was used for all the runs.

To obtain z_i's from the spiral soundings, plots of the virtual potential temperature Θ_v and mixing ratio Q versus altitude were produced. The z_i's can be fairly accurately determined as the top levels of the well-mixed layers. Figure 1(a) shows a typical plot, with the two corresponding soundings used for C12. It is noted, however, that Figure 1(a) shows a characteristic feature for all but one of the aircraft spiral soundings, namely that immediately on top of the mixed layer is an inversion layer which is composed of dry air. The one exception is the afternoon sounding for day M23, shown in Figure 1(b). This sounding was done immediately after the last 'run' on that day. This figure shows that there is an unstable layer composed of moist, cool air, residing on top of the warmer mixed layer. The effect of this instability will be discussed later when we deal with the covariance between θ and q, the fluctuations of potential temperature and of vapour mixing ratio, respectively.

2.2. Description of sites

The rugged-terrain site is centred over the Callide reservoir (24° 22′ S, 150° 38′ E) in Queensland, Australia; and the homogeneous site is over farm land (29° 53′ S, 149° 27′ E) to the southwest of Moree in New South Wales, Australia.

TABLE I

Instruments used

Quantities	Methods of measurement	Sampling rates (samples/second)	Maximum frequencies retained after numerical filtering (fast response) or averaging (slow resonse) (Hz)
Reference Temperatures			
– Dry bulb	'Rosemount' Platinum element, Ø 1.3 mm	5	0.25
– Wet bulb	'Rosemount' Platinum element, Ø 1.3 mm	5	0.25
Fast-response Temperatures			
– Dry bulb	Nickel wire, Ø 12.5 μm	100	10
– Wet bulb	Nickel wire, Ø 25.0 μm	100	10
Mixing ratio	Derived numerically from measurements of dry and wet bulb temperatures	5 and 100	0.25 and 10
Air vertical velocity fluctuation (artificially de-meaned)	Two angle-of-attack fixed vanes, fitted with *'Micro-measurement' strain gauges*	100	10
Air speed	Pitot tube, connected by a 3 m plastic tube to a 'Statham' pressure transducer-amplifier unit	100	0.25 and 10
Pressures (for heights)			
– Static	'Kistler' unit, model 314A	5	0.25
– Dynamic	'Kistler' unit, model 314D	100	10
Height above ground level	Radiometer	5	0.25
Surface temperature (not used here)		5	2.5

TABLE II

Observational details

Observation symbols	Location and date	Starting time of first and last runs	Number of runs	Mean aircraft air-speed	Duration of each run	Flight direction	Wind speed	Wind direction	Flight direction relative to wind direction	Number of Projected ground tracks	Cloud conditions	Ground conditions	Remarks
				m/s	min		m/s						
C12 Rugged terrain	Callide, 12/7/81	12.08 & 14.23	16	85.5	3	90°, 270°	1–2.5; mainly 1.5–2	190°–280°; mainly 210°–240°	oblique angle	1	clear sky	See text	
C13 Rugged terrain	Callide 13/7/81	11.25 & 13.29	16	85.5	3	90°, 270°	2–5; mainly 1–5	205°–255°; mainly 243°–255°	nearly parallel	1	clear sky	See text	
M23 Homog. terrain	Moree 23/11/83	11.34 & 13.22	13	79.5	3	180°, 360°	1.5–4.0; mainly 2.5–3.5	variable, 50°–140°	mainly perpendicular	4 parallel tracks at 1.5 km from one another	2/8 Cu to 4/8 Cu	Mainly harvested wheat field and medium vegetation in uncultivated land; some green *pasture* land; and brown-black ploughed land; patches of forested land	Some short-lived rain showers occurred near the observation site, and a brief shower occurred over the end of one ground track at one stage, ahead of the aircraft run
M29 Homog. terrain	Moree 26/01/82	14.08 & 14.43	6	79.2	3	30°, 210°	1–2	variable, but mainly 60°	nearly parallel	1	1/8 Cu	Similar to M23	

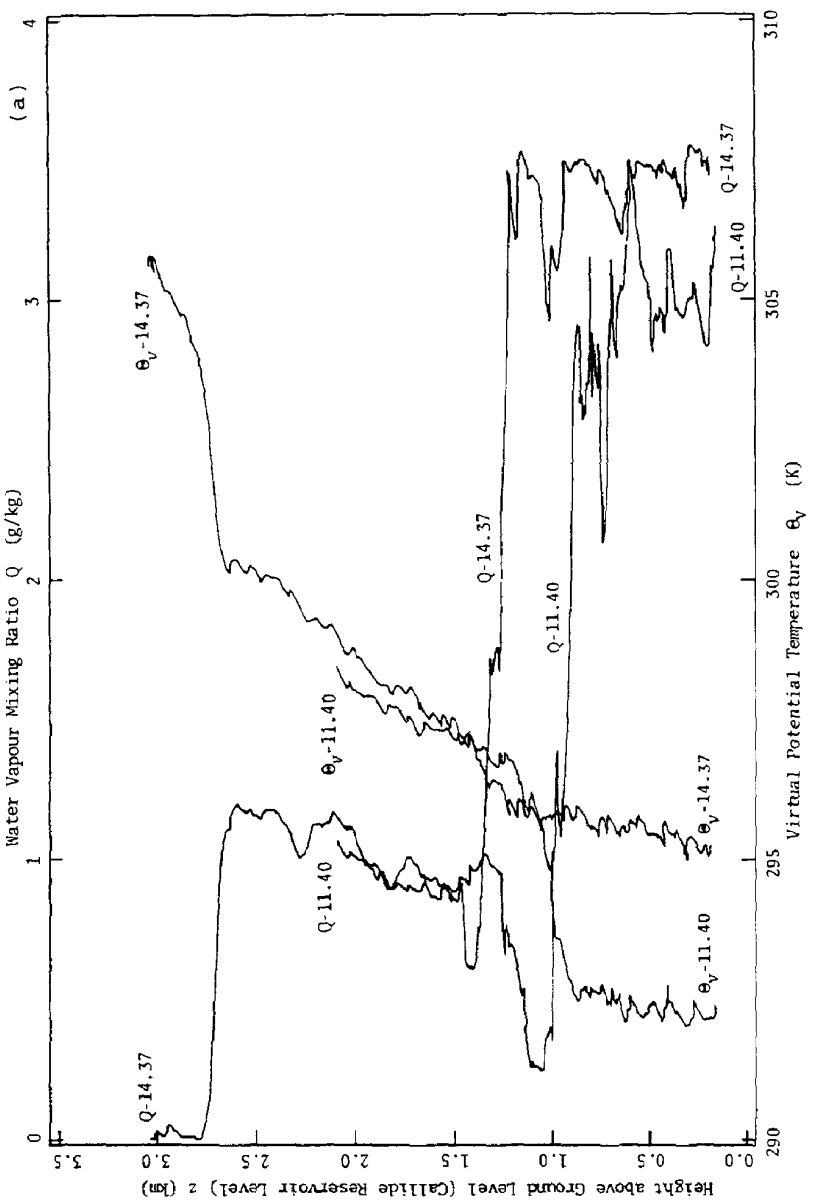

Fig. 1(a). Typical vertical profiles of virtual potential temperature Θ_v and mixing ratio Q obtained from aircraft spiral soundings. The heights of the mixed layer z_i can be readily read off as shown above. The two curves on the left are Θ_{v_i}; the Q curves are shown on the right. The soundings were made above Callide reservoir at 11.40 ($\Theta_{v_i} - 11.40$, $Q - 11.40$) and 14.37 ($\Theta_{v_i} - 14.37$, $Q - 14.37$).

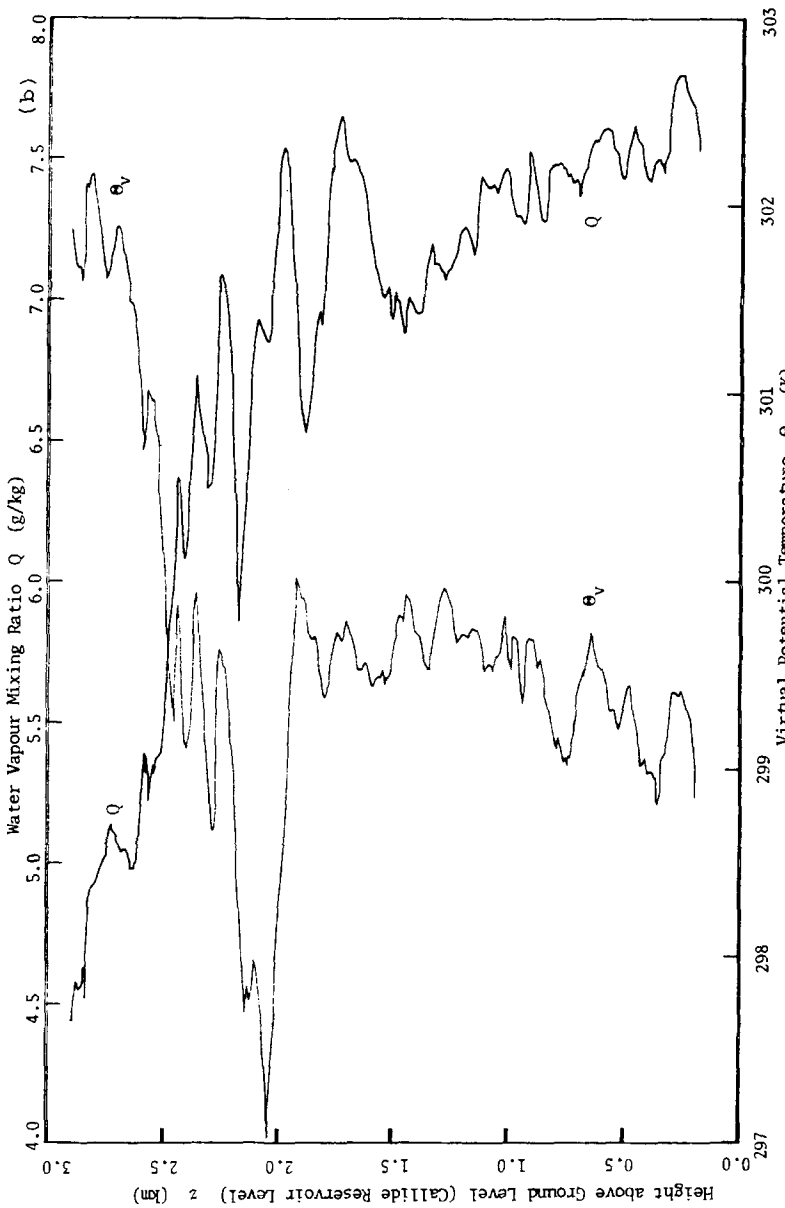

Fig. 1(b). Vertical profiles of virtual potential temperature Θ, and mixing ratio Q for the 'exceptional' day M23.

The Callide site is the western foothills of the Callide mountain range which runs NW–SE, with peaks rising to a maxium of about 900 m in the vicinity of the site. The Callide reservoir is at an altitude of 210 m AMSL; and all "heights above ground level" at the Callide site are measured relative to this altitude. To the West of the reservoir is the Bannana-Cooper mountain range, composed of more isolated hills with peaks rising to a maximum of about 500 m, and running parallel to the Callide range. The valley between the ranges, which is about 20 km wide near the reservoir, has its lowest altitude contour at about 140 m AMSL. The vegetation covering the area is typically scattered forest in the valley and on the Bannana-Cooper range, and medium to dense forest on the Callide range. Figure 2(a) shows a coarse contour map of the region and Figure 2(b) shows a coarse view of the Callide site.

The Moree site was typically flat, extensive farm land at various stages of cultivation and harvesting. Isolated patches of forest can also be seen but there is no significant land mark in the region. The average altitude is 180 m AMSL. Some more details about the ground conditions can be seen in Table II.

2.3. Data processing

Measurements were collected *in situ* on magnetic tapes at the rates of 100 samples/s for 'fast' data, and 5 for 'slow' data. Because the various instruments were mounted at different locations, and have different response time delays, care has been taken to ensure that all relevant signals are synchronised. The fast data have been numerically filtered via a Fast Fourier Transform (FFT) scheme to give a maximum frequency of 10 Hz. Most of the slow data are, however, averaged to give 2-s averages. Table I gives some further details about the variables involved. The 10 Hz time series after being linearly detrended were used to obtain various statistics. The computers involved were a ROLM for data collection, a Cyber 76 for processing and a VAX 11/750 for statistical analysis.

As shown in Table II, each 'run' lasted about 3 min. Assuming Taylor's hypothesis of frozen turbulence, and with a typical aircraft airspeed of 80 m/s, this gives maximum wavelengths of about 14 km. The number of useful data points per time series is, however, only about 3300, corresponding to 165 s of data sampling in the mid-section of the time series.

For computations involving spectra, such as those for the peak wavelengths of the vertical velocity fluctuations or tne dissipation rate of kinetic energy, a FFT scheme is used.

The computation of co-variances and variances are performed by the eddy correlation method. The variance of air speed fluctuation v is treated differently, however. In this case, due to the resonant effect in the 3 m long plastic tube connecting the Pitot tube and the transducer-amplifier unit, there is a significant lifting at the high frequency end of the response curve of the probe. Therefore, the variance of v is calculated from

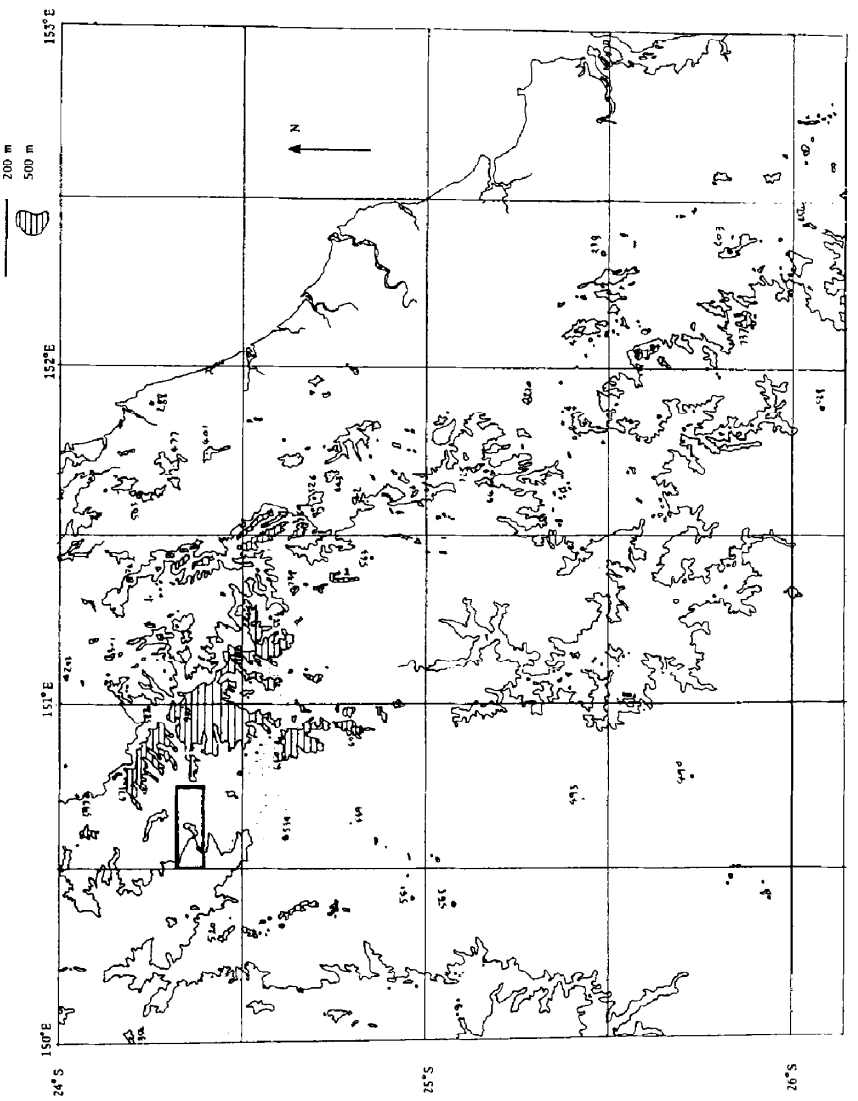

Fig. 2(a). A contour map of the Callide region. The heavy-lined rectangle corresponds to the Callide site shown in Figure 2b.

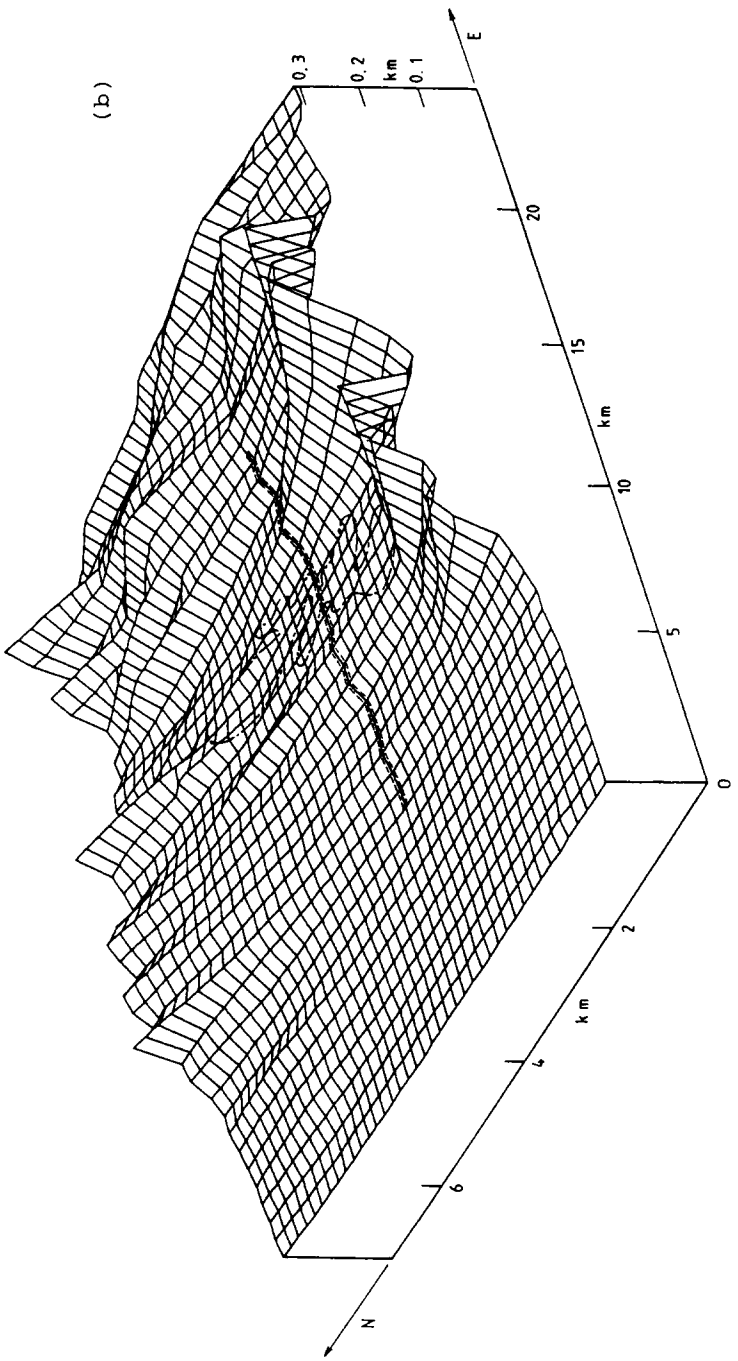

Fig. 2(b). A coarse view of the Callide site, corresponding to the heavy-lined rectangle in Figure 2(a). Here the origin 0 is set at the mean sea level point of (24° 23′ 13″ S, 150° 30′ 00″ E2. ▬▬▬▬▬▬▬▬ : projected ground track. —— – —— – —— : approximate boundary of the Callide reservoir.

$$\overline{v^2} = \int_{f_{min}}^{f_{max}} S_v(f)\, df,$$

where f is the frequency and S_v is the corrected spectra of v. The corrected variance is, however, only about 11% lower than the uncorrected one at the high frequency end.

For temperatures, on the other hand, there are some attenuations in the probes' frequency response at frequencies above 3 Hz. The errors involved are, however, small, and the temperature variances are expected to be low by less than 5% for the Callide data, and less than 2% for the Moree data. Assuming no significant phase shifts between the relevant parameters, the heat fluxes and temperature-mixing ratio co-variances are also expected to be fairly accurate.

3. Results

3.1. Scaling factors

In a steady convective mixed layer, it has been amply shown (Deardorff, 1970; Kaimal *et al.*, 1976; Wyngaard *et al.*, 1978; Guillemet *et al.*, 1983; etc.) that the appropriate scaling factors are (for notation, see Appendix)

$$\begin{aligned} &z_i\, \theta_* = \overline{(w\theta)_0}/w_* \\ &w_* = (g\overline{(w\theta)_0} z_i/\Theta)^{1/3} \quad q_* = \overline{(wq)_0}/w_* . \end{aligned} \tag{1}$$

We adopt (1) in this report. Here, the ground fluxes $\overline{(w\theta)_0}$ and $\overline{(wq)_0}$ are obtained by extrapolation from the values obtained at higher levels.

In the following, we show our results, often against the background of results published by other workers. Extensive comparison is made with the data of Druilhet *et al.* (1983a,b); therefore, a note should be made: their data were collected in more rugged terrain, under stronger wind conditions.

3.2. Co-variances and correlation coefficients

The vertical profiles of the normalised co-variance $\overline{w\theta}/\overline{(w\theta)_0}$ representing normalised sensible heat flux are shown in Figure 3(a). There seems to be no discernible difference between the rugged terrain profile and that over homogeneous terrain. Our values are similar to the AMTEX data of Wyngaard *et al.* (1978), and the Ashchurch–Minnesota data of Caughey and Palmer (1979), but somewhat lower than those obtained by Lenschow (1974), or Druilhet *et al.* (1983a) for homogeneous terrain conditions. Our rugged terrain data also lack the irregularities shown in Druilhet *et al.*'s rugged terrain data.

The correlation coefficients $r_{w\theta}$ between w and θ are shown in Figure 3(b). Like the normalised sensible heat flux, there is no recognisable difference between the cases for rugged and smooth terrain. Also, our data seemed to show a tendency

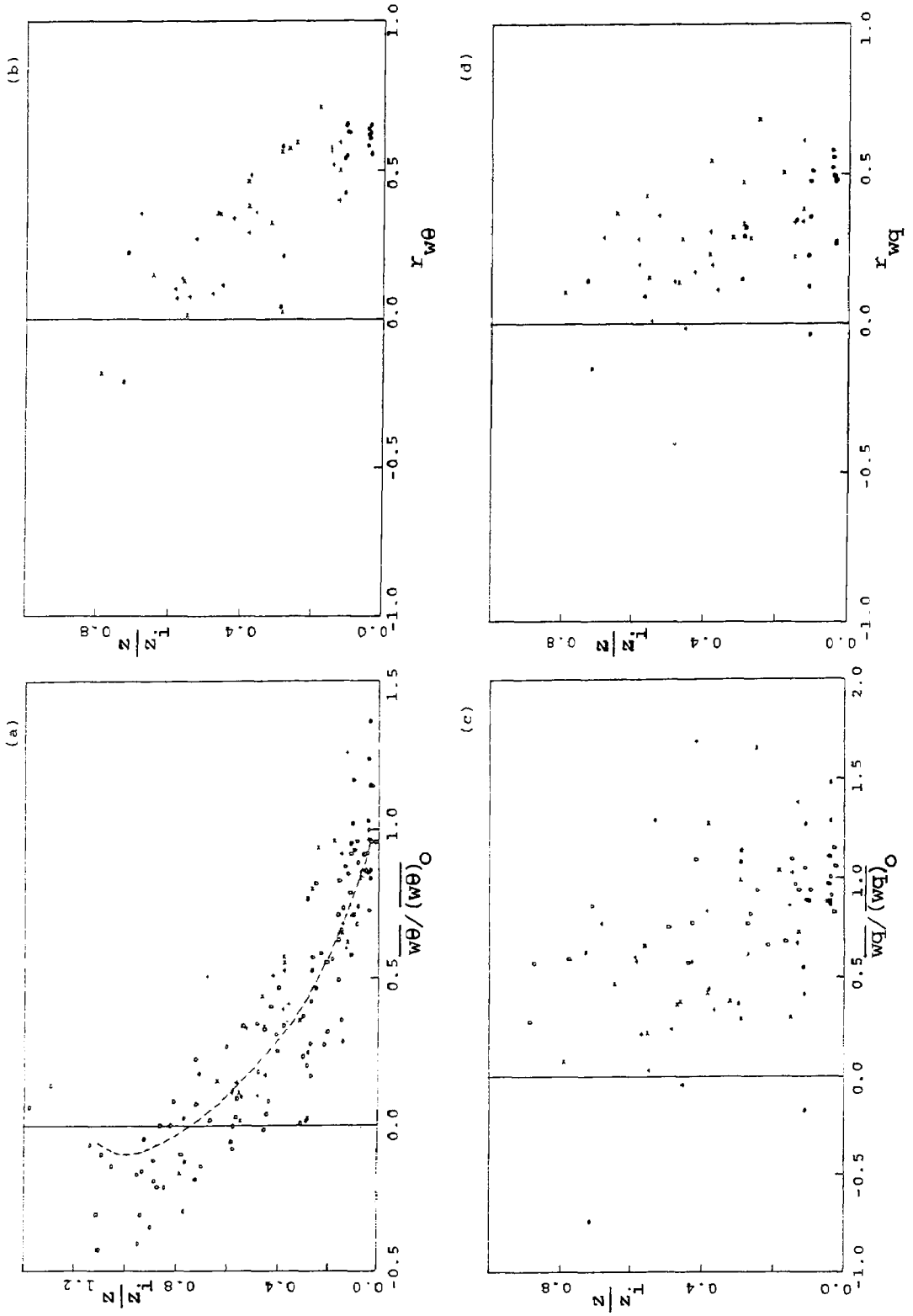
(a)
(b)
(c)
(d)
z_i/z
r_wθ
r_bm
O(θm)/(wθ)
O(bm)/(wb)

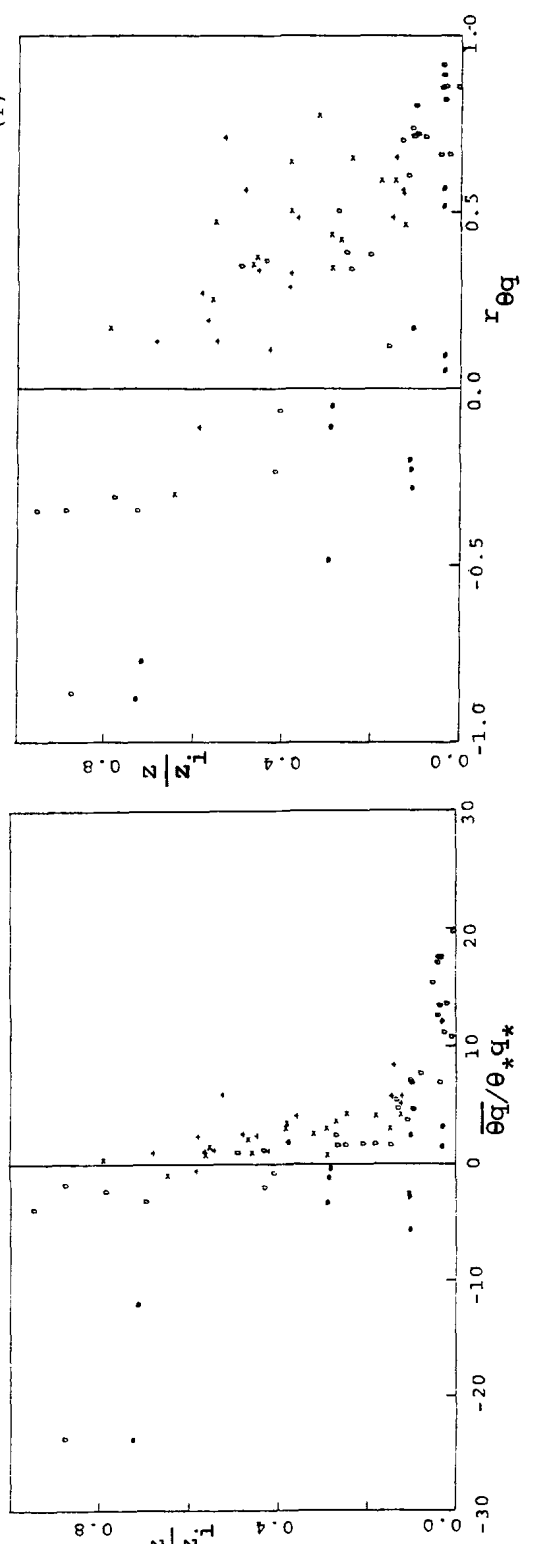

Fig. 3. (a) Normalised kinematic heat flux $h_* = \overline{w\theta}/(\overline{w\theta})_0$ versus normalised height $z_* = z/z_i$ above ground level. Rugged terrain data: +, C12 (see Table II for observation symbols); ×, C13. Homogeneous terrain data: ●, M23; ◓, M29; ○, from Wyngaard *et al.* (1978); ○: from Caughey and Palmer (1979); ----, Deardorff's (1972) presentation of Lenschow's (1970) aircraft results. (b) $r_{w\theta}$ versus z/z_i. Symbols are the same as in Figure 3(a). (c) Normalised moisture flux $\overline{wq}/(\overline{wq})_0$ versus z/z_i. Symbols are the same as in Figure 3(a). (d) r_{wq} versus z/z_i. Symbols are the same as in Figure 3(a). (e) Normalised covariance $\overline{\theta q}/(\theta_* q_*)$ versus z/z_i. Symbols are the same as in Figure 3(a). (f) $r_{\theta q}$ versus z/z_i. Symbols are the same as in Figure 3(a).

for $r_{w\theta}$ to stay constant up to $z/z_i \doteq 0.1$ only, compared to 0.3 as suggested by the results of Druilhet *et al.* (1983a). Our $r_{w\theta}$ value at ground level is, however, similar to the homogeneous terrain ground level value of Druilhet *et al.*, namely about 0.6.

Figures 3(a) and 3(b) also show that, from our data, zero heat flux occurs at a level of $z/z_i \doteq 0.7$. This level is comparable to that obtained by Wyngaard *et al.* (0.67), but lower than those of Lenschow (0.87), or Druilhet *et al.* (0.81).

Profiles of the normalised moisture flux $\overline{wq}/\overline{(wq)_0}$ are shown in Figure 3(c). Despite large scatter, the data still show recognisable decreasing trends with height. The trends for the rugged and smooth terrain are perhaps similar, but steeper than that obtained from AMTEX data (Wyngaard *et al.*, 1978). In Figure 3(d), it can be seen that the correlation coefficient r_{wq} also shows similar trends over rugged and smooth terrain, but with rugged terrain values slightly higher. Our data do not show the constancy of r_{wq} with height, as found by Druilhet *et al.* (1983). Also, our projected ground values of r_{wq} are somewhat higher (0.4 for smooth terrain, and 0.5 for rugged terrain) than those shown in the paper of Druilhet *et al.*

Figures 3(e) and 3(f) show the vertical profiles of the normalised co-variance $\overline{\theta q}/\theta_* q_*$ and the correlation coefficient $r_{\theta q}$. The smooth-terrain data of M23 show a strong anti-correlation between θ and q for most of the upper part of the mixed layer. In fact, a positive correlation occurs only for $z/z_i < 0.2$. This value is much smaller than the value 0.5 obtained from the observations of Druilhet *et al.* (1983a) or the value 0.6 obtained by Deardorff's (1974) numerical simulation. It should be noted, as shown in Table II, that on day M23, the observational site was covered with extensive cumulus cloud, and there were even some short showers. The result is that, as revealed in the afternoon sounding for day M23 shown in Figure 1(b), there was an unstable layer composed of moist, cool air residing on top of the warmer mixed layer. It is the entrainment of the moist, cool layer of air into the mixed layer that causes such deep penetration and results in negative values of $r_{\theta q}$ being observed down to such low levels. This mechanism is more effective than and different from the 'normal' entrainment where dry, warm air in the stable inversion layer is entrained into the cooler mixed layer. This latter mechanism is found in the works of Druilhet *et al.*, Deardorff, and in our data over rugged terrain.

Over rugged terrain, the values of $\overline{\theta q}/(\theta_* q_*)$ seem to collapse well, and stay positive, although small, for most of the lower part of the mixed layer. The cross-over point to negative values occurs probably at about $0.7 z_i$. This rather high level, when compared with homogeneous terrain data of Druilhet *et al.* ($0.5 z_i$) and Deardorff's simulation ($0.6 z_i$), is thought to be due to the advective effects of the underlying topography, which preserve the long wavelength components of the convective structures associated with warm, moist air rising from the ground, and limit the entrainment effect to the top 30% of the mixed layer. The correlation coefficient $r_{\theta q}$, on the other hand, seems to stay fairly constant at about 0.55, up

to $z/z_i = 0.3$, then decreases linearly with height. This is in contrast to the data of Druilhet *et al.*, which show $r_{\theta q}$ over rugged terrain to be small, negative, and nearly constant for the whole of the mixed layer ($r_{\theta q} = -0.1$).

3.3. Variances

Figure 4(a) shows vertical profiles of the normalised variance of the vertical velocity fluctuation $\overline{w^2}/w_*^2$.

There does not seem to be any significant difference between the rugged terrain

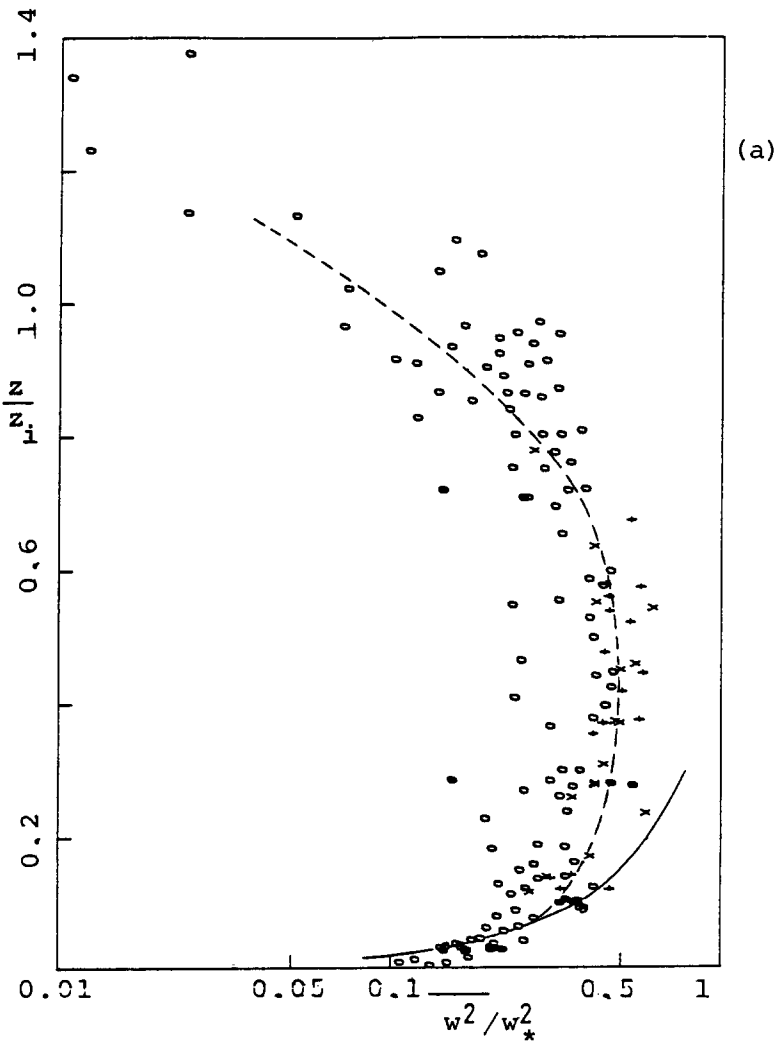

Fig. 4(a). Normalised variance of the vertical velocity fluctuation $\overline{w^2}/w_*^2$ versus z/z_i. ————: free convection formulation for the surface layer, $\overline{w^2}/w_*^2 = 1.8\ (z/z_i)^{2/3}$, by Wyngaard *et al.* (1971); — — — — — —: The average of the S_1 and S_2 cases in Willis and Deardorff's (1974) laboratory results, as presented by Caughey and Palmer (1979). Other symbols are the same as in Figure 3(a).

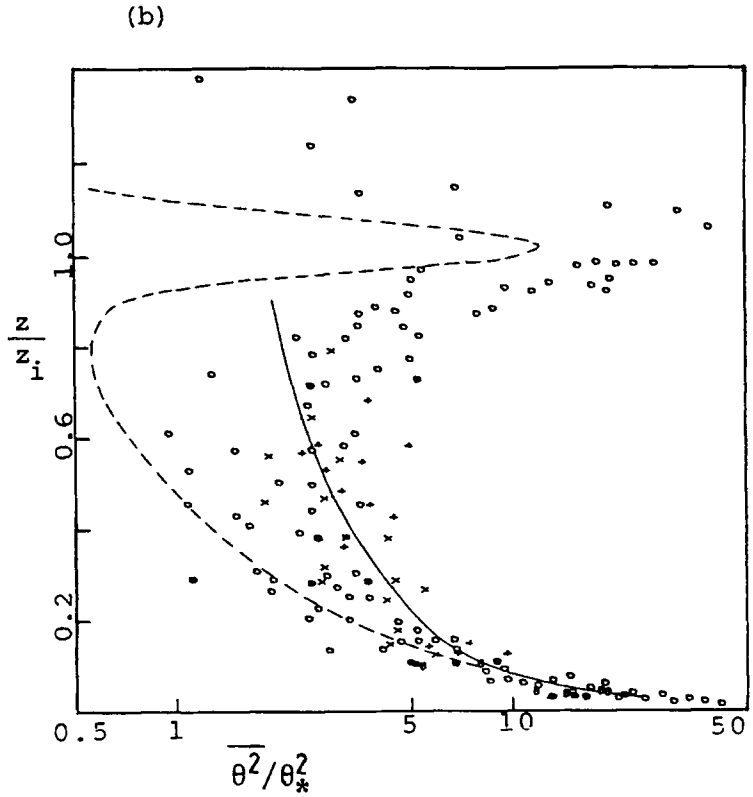

Fig. 4(b). Normalised variance of the potential temperature $\overline{\theta^2}/\theta_*^2$ versus z/z_i. ————: free convection formulation, $\overline{\theta^2}/\theta_*^2 = 1.8(z/z_i)^{-2/3}$ by Wyngaard *et al.* (1971); — — — — —: The S_1 case in Willis and Deardorff's (1974) laboratory results. Other symbols are the same as in Figure 3(a).

and the homogeneous terrain data, except in the upper part of the mixed layer, where the few data points available seem to suggest that the homogeneous terrain values are smaller. Overall, $\overline{w^2}/w_*^2$ increases quickly with height near the ground, reaches a maximum value of about 0.5 at $z/z_i \doteq 0.5$, before starting to decrease again. The homogeneous terrain data follow well the free convection prediction of Wyngaard *et al.* (1971) which is $1.8(z/z_i)^{2/3}$, up to $z/z_i \doteq 0.1$. In the middle part of the mixed layer, all data seem to agree with the laboratory average results of Willis and Deardorff (1974) as presented by Caughey and Palmer (1979) whose own data, however, have lower values than ours.

Profiles of the normalised variance of potential temperature, $\overline{\theta^2}/\theta_*^2$, are shown in Figure 4(b). Again, rugged terrain and homogeneous terrain data do not show any substantial difference, except that the rugged terrain values are perhaps slightly larger than the homogeneous terrain ones for $z < 0.4z_i$. Compared to the data obtained by Caughey and Palmer (1979), and the aircraft data assembled by Willis and Deardorff (1974) (not shown), our data agree well in the surface layer

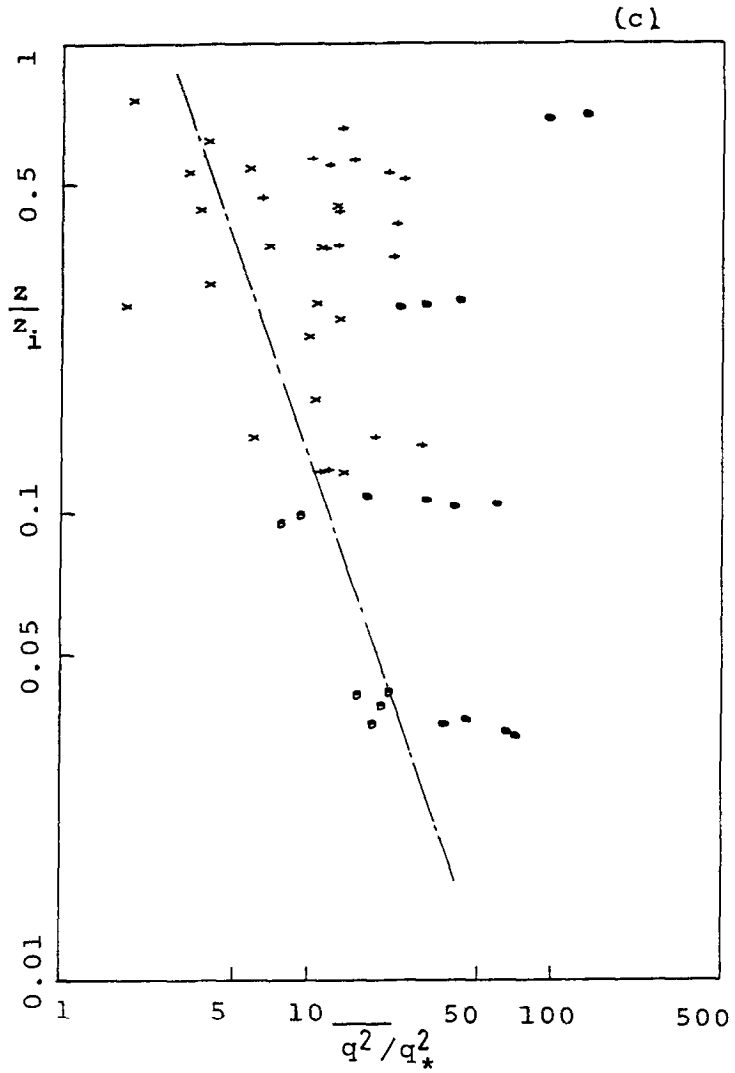

Fig. 4(c). Normalised variance of the mixing ratio $\overline{q^2}/q_*^2$ versus z/z_i; ——– – ——– – ——: free convection formula $\overline{q^2}/q_*^2 = 2.59(z/z_i)^{-2/3}$, by Smedman-Högström (1973). Other symbols are the same as in Figure 3(a).

$(z/z_i < 0.1)$, but become slightly larger at higher levels. In the surface layer, the data follow the $(z/z_i)^{-2/3}$ law, but with a coefficient of about 1.5 instead of 1.8 as predicted by the free convection formulation (Wyngaard *et al.*, 1971). The minimum value for $\overline{\theta^2}/\theta_*^2$ is about 0.3, and occurs at $z/z_i \doteq 0.5$, the same level as the maximum value of $\overline{w^2}/w_*^2$.

Figure 4(c) shows that the variance of the mixing ratio q does not seem to follow a simple scaling scheme, as used here. An attempt at using an interfacial scaling scheme similar to the one proposed by Tuzet *et al.* (1983) did not seem to help

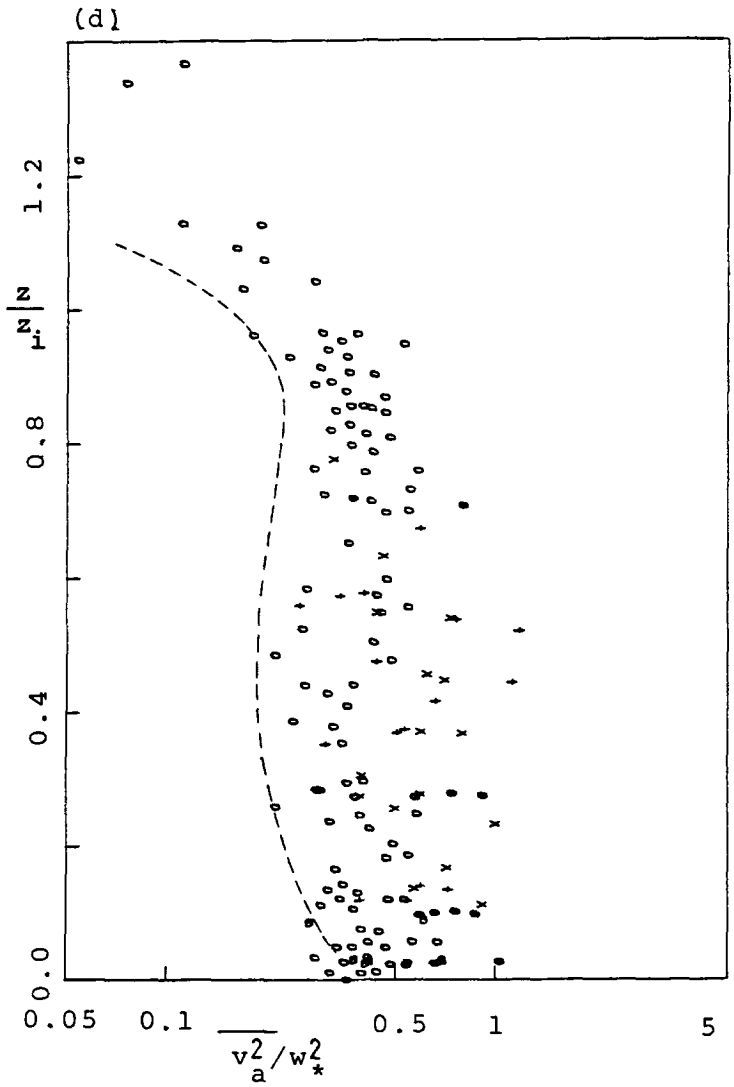

Fig. 4(d). Normalised variance of the aircraft airspeed fluctuation $\overline{v_a^2}/w_*^2$ versus z/z_i. — — — — — —: the average of the S_1 and S_2 cases in Willis and Deardorff's (1974) laboratory results, as presented by Caughey and Palmer (1979). Other symbols are the same as in Figure 3(a).

very much in collapsing the data either, perhaps because of uncertainties in the values of $\delta\Theta/\delta z$ and $\delta Q/\delta z$ immediately above z_i in some data. However, the smooth-terrain data M23 show that an entrainment effect can be felt as far down as $z/z_i \doteq 0.2$, consistent with the $\theta - q$ covariance result shown in Figure 3(e). The C13 and M29 sets of data, taken together, seem to be the only ones which have some similarity with the free convection formulation of Smedman-Högström (1973). The C12 data, however, do not show significant variation with height.

On most of the data collection runs, the aircraft flight paths were either at small angles to, or perpendicular to the wind directions. Therefore the fluctuations v_a in airspeed approximately correspond to the longitudinal or transversal fluctuations in the wind speed, u and v, respectively. Figure 4(d) shows the normalised variance $\overline{v_a^2}/w_*^2$. Again, there does not seem to be any significant difference between the rugged-terrain and homogeneous terrain. The M23 homogeneous-terrain data, however, seem to indicate some slight decrease with height. Taking all data together, $\overline{v_a^2}/w_*^2$ seems to be constant with height and to fluctuate about 0.55. Caughey and Palmer (1979) also obtained a similar distribution of $\overline{u^2}/u_*^2$ and $\overline{v^2}/w_*^2$ with height, but on average, their data are smaller, having a mean of 0.4.

3.4. Peak wavelengths

The peak wavelengths are defined here as the wavelengths corresponding to the maximum values of $kS_x(k)$ in the x variable. Here, Taylor's frozen turbulence hypothesis has been asumed, so that $k = f/V_a$, where f is the frequency measured in the aircraft's frame of reference, and V_a is the aircraft air speed.

The peak wavelengths $(\lambda_m)_w$ from the spectra of the vertical velocity fluctuation w are shown in Figure 5(a). Again, there does not seem to be any substantial difference between homogeneous-terrain and rugged-terrain data, except that the latter show more scatter due to the interaction of turbulence with the underlying terrain. Despite the scarcity and large scatter of the rugged-terrain data in the upper region, the tendency for $(\lambda_m)_w$ to decrease with height above $z/z_i \doteq 0.5$ is still recognisable. Our data therefore seem to be similar to those obtained by Caughey and Palmer, and to the lower part ($z/z_i < 0.5$) of the results of Kaimal *et al.* (1976). Druilhet *et al.* (1983a) also obtained similar results over homogeneous terrain; however, our data do not seem to show smaller values over rugged terrain as theirs do. Figure 5(a) shows that the maximum value of $(\lambda_m)_w$ is about 1.5 z_i and occurs at $z/z_i \doteq 0.5$.

For the potential temperature fluctuation θ, the peak wavelengths $(\lambda_m)_\theta$ are more difficult to obtain, due to low frequency variations from run to run. However, approximate peaks in the $kS_\theta(k)$ plots can still be identified to give $(\lambda_m)_\theta$ as shown in Figure 5(b). Despite large scatter, it still can be seen that $(\lambda_m)_\theta$ increases quickly with height in the surface layer, then approaches a steady value of about $2z_i$ for $z/z_i > 0.5$. There does not seem to be a tendency for $(\lambda_m)_\theta$ to decrease at higher levels, as $(\lambda_m)_w$ does. This is to be compared with the data of Kaimal *et al.* (1976) which show that as z approaches 0.1 z_i, $(\lambda_m)_\theta$ approaches the characteristic wavelength 1.5 z_i, the same as the maximum value of $(\lambda_m)_w$. Thus, the vertical profile of $(\lambda_m)_\theta$ from our data changes more gradually than that of Kaimal *et al.* (see Figure 5(b)).

Again, there does not seem to be any systematic difference between the rugged- and homogeneous-terrain data shown here, except that the rugged-terrain data show more scatter.

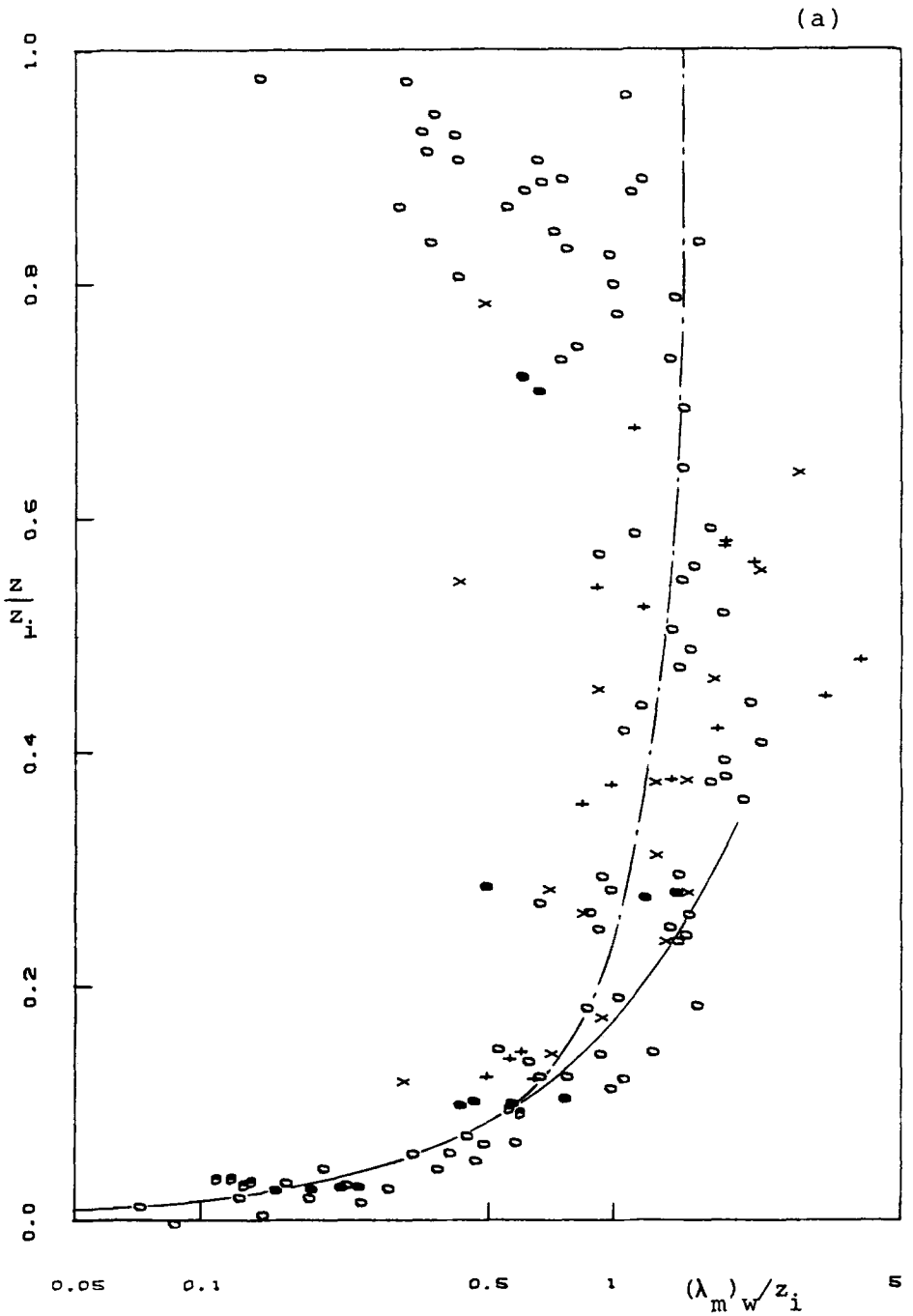

Fig. 5(a). Normalised peak wavelength $(\lambda_m)_w/z_i$ of the w spectra, versus z/z_i. ————: free convection formulation $(\lambda_m)_w/z_i = 5.9\ z/z_i$, $z < 0.1 z_i$, by Kaimal *et al.* (1976): —— - —— - ——: the results of Kaimal *et al.* for the region $0.1 < z/z_i < 1.0$. Other symbols are same as in Figure 3(a).

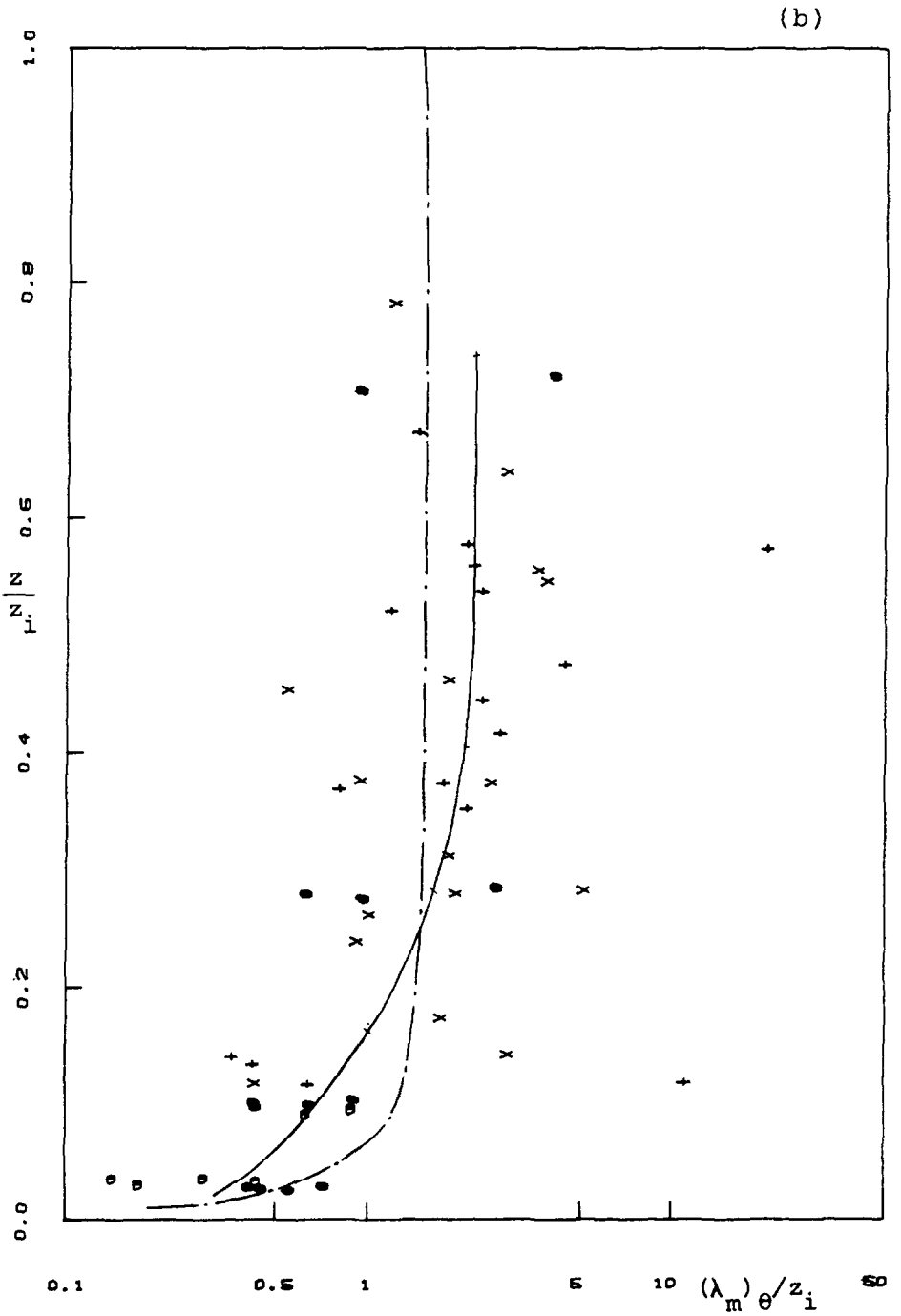

Fig. 5(b). Normalised peak wavelength $(\lambda_m)_\theta/z_i$ of the θ spectra versus z/z_i; ————————: curve fitting of data by eye; — — — — — — — —: the results of Kaimal *et al.* Other symbols are same as in Figure 3(a).

3.5. Dissipation rates

The rates of dissipation of turbulent kinetic energy ϵ, temperature variance N_θ, and mixing ratio variance N_q, are estimated from the inertial subrange of one-dimensional spectra of fluctuations in vertical velocity, temperature and mixing ratio, respectively. Assuming the frozen turbulence hypothesis, the useful relations are

$$f^{5/3} \cdot S_w(f) = \frac{4}{3}\alpha_u \left(\frac{V_a}{2\pi}\right)^{2/3} \epsilon^{2/3}; \quad \alpha_u = 0.5$$

$$f^{5/3} \cdot S_\theta(f) = \alpha_\theta \left(\frac{V_a}{2\pi}\right)^{2/3} \epsilon^{-1/3} N_\theta; \quad \alpha_\theta = 0.8$$

$$f^{5/3} \cdot S_q(f) = \alpha_q \left(\frac{V_a}{2\pi}\right)^{2/3} \epsilon^{-1/3} N_q; \quad \alpha_q = 0.8.$$

Here, we adopt the numerical values of α_u, α_θ and α_q from Druilhet *et al.* (1983b).

Figure 6(a) shows the vertical distribution of normalised ϵ, defined here as $\epsilon_* = \epsilon \cdot z_i / w_*^3$. The rugged and homogeneous terrain data do not show any significant difference. Our data show a rapid decrease of ϵ_* with height, up to $z/z_i \doteq 0.2$, then an almost constant value at about 0.24, right up to $z \doteq 0.8\ z_i$ which is the highest level in our data set. In this way, Guillemet *et al.* (1983), and Caughey and Palmer (1979) have obtained similarly constant results, but with large values. For the bulk of the mid-section of the mixed layer, the data of Guillemet *et al.* are between 0.35 and 0.65, while the data of Caughey and Palmer are between about 0.51 and 0.77, as shown in Figure 6(a). On the other hand, the homogeneous-terrain data of Druilhet *ét al.* (1983a) show that ϵ_* decreases at a much larger, and constant, rate with respect to height. Below $z \doteq 0.7 z_i$, their rugged-terrain data also show similar, but somewhat weaker behavior.

The vertical profile of the normalised dissipation rate of the temperature variance, defined here as $(N_\theta)_* = N_\theta z_i / w_* \theta_*^2$, is shown in Figure 6(b). Here the rugged terrain values are slightly larger than those over homogeneous terrain, for z below about $0.4 z_i$; but overall, there is no substantial difference between the two sets of data. This is similar to the behaviour of $\overline{\theta^2}/\theta_*^2$ shown in Figure 4(b). Our data seem to follow closely the profile of data obtained by Caughey and Palmer (1979), except that our value of $(N_\theta)_*$ is smaller, as shown in Figure 6(b). Also, in the lower levels ($z/z_i < 0.5$), our data seem to agree fairly well with the $(z/z_i)^{-4/3}$ law predicted under the local free convection similarity hypothesis (Wyngaard, 1973). The dashed line in Figure 6(b) represents the relation:

$$(N_\theta)_* = A_\theta (z/z_i)^{-4/3}$$

where the constant $A_\theta = 0.4$ is estimated by eye-fitting the observational points.

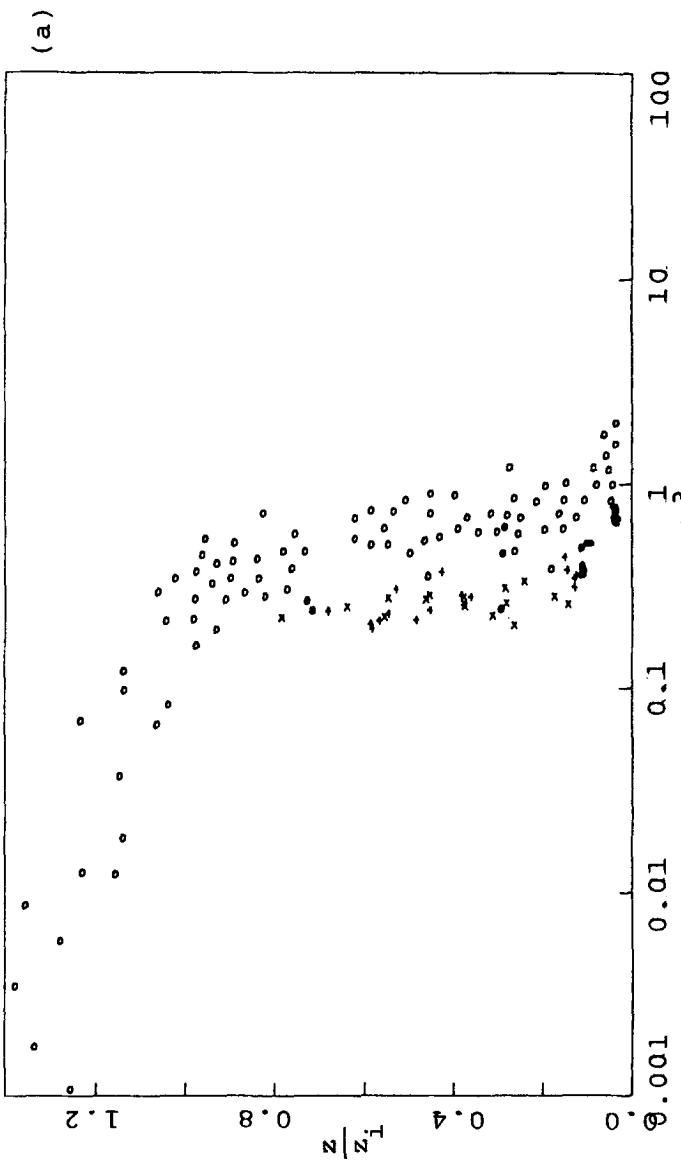

Fig. 6(a). Normalised dissipation rate of turbulent kinetic energy $\epsilon z_i/w_*^3$ versus z/z_i. Symbols are the same as in Figure 3(a).

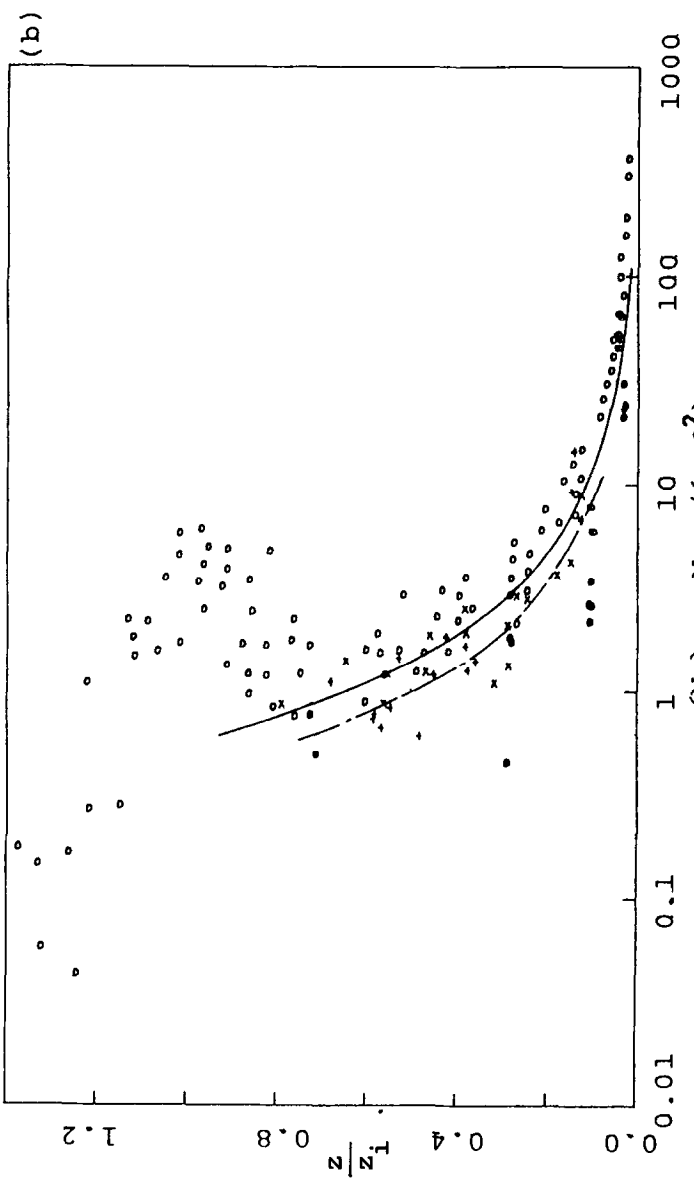

Fig. 6(b). Normalised dissipation rate of temperature variance, $(N_\theta)_* = N_\theta z_i/w_*\theta_*^2$ versus z/z_i. ——————: the smooth terrain formulation of Guillemet *et al.* $(N_\theta)_* = 0.55(z/z_i)^{-4/3}$; —— - —— - ——: curve fitting of data by eye $(N_\theta)_* = 0.4(z/z_i)^{-4/3}$. Other symbols are the same as in Figure 3(a).

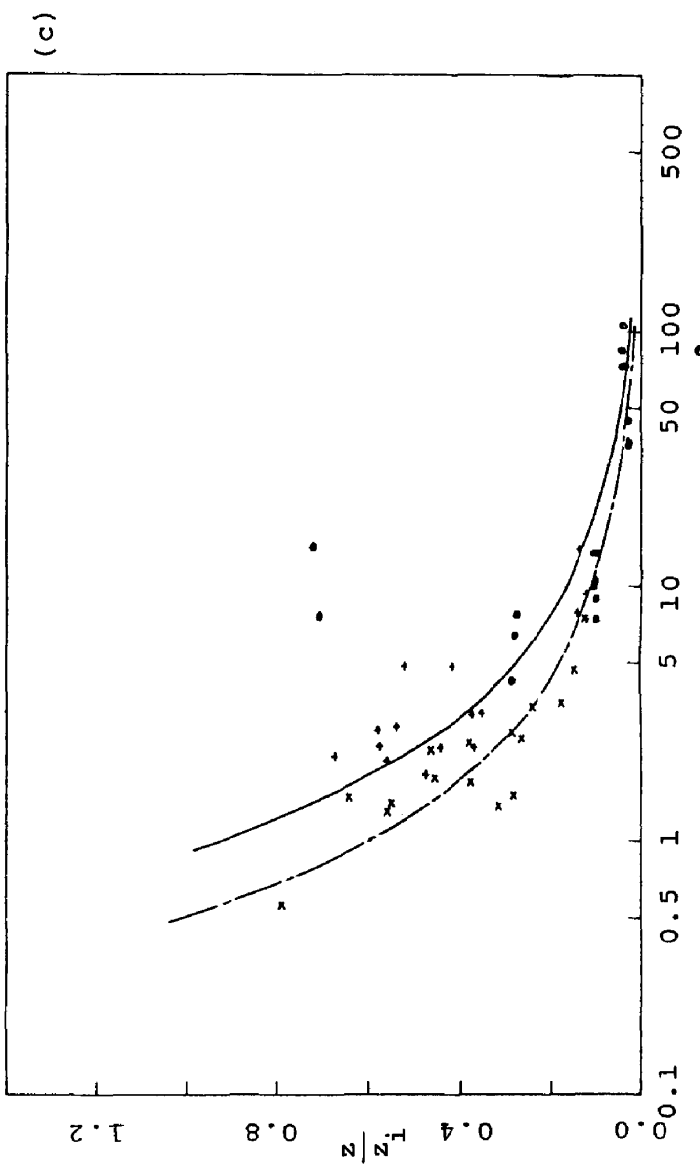

Fig. 6(c). Normalised dissipation rate of mixing ratio variance $(N_q)_* = N_q z_i/w_* q_*^2$ versus z/z_i; ——————: the smooth terrain formulation of Guillemet *et al.* $(N_q)_* = 0.9(z/z_i)^{-4/3}$; — — — —: curve fitting of data by eye $(N_q)_* = 0.5(z/z_i)^{-4/3}$. Other symbols are the same as in Figure 3(a).

The present value of A_θ is somewhat smaller than the 0.55 value given by Guillemet *et al.* (1983).

Figure 6(c) shows the vertical profile of the normalised dissipation rate of the mixing ratio variance, $(N_q)_* = N_q z_i / w_* q^{*2}$. Some similarity can be seen with the profiles of $\overline{q^2}/q_*^2$ shown in Figure 4(c). The entrainment effect in the M23 set of data can still be seen to be effective as far down as $z \doteq 0.2 z_i$; and the C13 set of data, together with the data points below $z \doteq 0.1 z_i$ in the homogeneous terrain cases show the free convection behaviour of $A_q (z/z_i)^{-4/3}$. However, our value of $A_q = 0.5$, obtained by eye-fitting the data points, is smaller than the 0.9 value given by Guillemet *et al.* (1983).

4. Concluding Remarks

Overall, our data do not show any marked difference in the turbulence statistics between homogeneous and rugged terrain, except for those related to the mixing ratio q as shown in Figures 3(e), 3(f), 4(c) and to a milder degree in Figure 3(d). The differences between homogeneous and rugged-terrain data shown in these figures are, however, believed to be due to the entrainment effects from the layers above z_i, and thus dependent more on the conditions in these layers, than on the underlying terrain. In this way, our results are very different from those obtained by Druilhet *et al.* (1983a), who have shown substantial variations between data collected over homogeneous and rugged terrain. One way to explain the differences between our results and Druilhet *et al.*'s is that on the two days in which the C12 and C13 sets of data were collected, the wind was light and was mainly from the SW to WSW (see Table II). Since to the west and south of the observational site, as shown in Figures 2(a) and 2(b), the terrain is somewhat less rugged than that studied in the paper of Druilhet *et al.* (see Noilham *et al.* (1983) for a description of their experimental site), the terrain-induced turbulence in our data is not strong enough to cause any large deviation from the homogeneous-terrain cases, except for larger scatter in the data points. Thus, our data show that results from homogeneous-terrain experiments are still valid for terrain with some degree of ruggedness, at least to the extent encountered in this report.

Appendix

Notation

Θ	mean potential temperature of the mixed layer (K)
θ	potential temperature fluctuation (K)
w	vertical velocity fluctuation (m/s)
v	aircraft airspeed fluctuations, along the flight direction (m/s)
z	height above ground level (m)
z_i	height above ground level of the mixed layer (m)
q	water vapour mixing ratio (g/kg)
g	gravitational constant (m/s^2)
S_x	spectra of variable x

f frequency (Hz)
k wave number (cycle/m)
r_{xy} correlation coefficient between variable x and y
$(\lambda_m)_x$ maximum wavelength of variable x, i.e. the wavelength at the maximum value of $S_x(f)$ (*m/cycle*)

Subscripts
0 at ground surface
* for normalising factors
a for aircraft

References

Caughey, S. J. and Palmer, S. G.: 1979, 'Some Aspects of Turbulence Structure through the Depth of the Convective Layer', *Quart. J. Roy. Meteor. Soc.* **105**, 811–827.

Deardorff, J. W.: 1970, 'Convective Velocity and Temperature Scales for the Unstable Planetary Boundary Layer and for Rayleigh Convection', *J. Atmos. Sci.* **27**, 1211–1213.

Deardorff, J. W.: 1974, 'Three-Dimensional Numerical Study of Turbulence in an Entraining Mixed Layer', *Bound.-Layer Meteor.* **7**, 199–226.

Druilhet, A., Noilham, J., Benech, B., Dubosclard, G., Guedalia, D., and Frangi, J.: 1983a, 'Étude Expérimentale de la Couche Limite au-desus d'un Relief Modéré Proche d'une Chaîne de Montagne', *Boundary-Layer Meteorol.* **25**, 3–16.

Druilhet, A., Frangi, J. P., Guedalia, D., and Fontan, J.: 1983b, 'Experimental Studies of the Turbulence Structure Parameters of the Convective Boundary Layer', *J. Climate Appl. Meteorol.* **22**, 594–608.

Guillemet, B., Isaka, H., and Mascart, P.: 1983, 'Molecular Dissipation of Turbulent Fluctuations in the Convective Mixed Layer. Part 1: Height Variations of Dissipation Rates', *Boundary-Layer Meteorol.* **27**, 141–162.

Kaimal, J. C., Wyngaard, J. C., Haugen, D. A., Coté, O. R., and Izumi, Y.: 1976, 'Turbulence Structure in the Convective Boundary Layer', *J. Atmos. Sci.* **33**, 2152–2169.

Kaimal, J. C., Eversole, R. A., Lenschow, D. H., Stankov, B. B., Kahn, P. H., and Businger, J. A.: 1982, 'Spectral Characteristics of the Convective Boundary Layer over Uneven Terrain', *J. Atmos. Sci.* **39**, 1098–1114.

Lenschow, D. H.: 1974, 'Model of the Height Variation of the Turbulence Kinetic Energy Budget in the Unstable Planetary Boundary Layer', *J. Atmos. Sci.* **31**, 465–474.

Noilham, J., Benech, B., Druilhet, A., and Dubosclard, G.: 1983, 'Étude Expérimentale de la Couche Limite au-dessus d'un Relief Modéré Proche d'une Chaîne de Montagne', *Boundary-Layer Meteorol.* **24**, 395–414.

Panofsky, H. A., Larko, D., Lipschutz, R., Stone, G., Bradley, E. F., Bowen, A. J., and Hoistrup, J.: 1982, 'Spectra of Velocity Components over Complex Terrain', *Quart. J. Roy. Meteor. Soc.* **108**, 215–230.

Smedman-Högström, A. S.: 1973, 'Temperature and Humidity Spectra in the Atmospheric Surface Layer', *Boundary-Layer Meteorol.* **3**, 329–347.

Tuzet, A., Guillemet, B., and Isaka, H.: 1983, 'Echelles Interfaciales des Fluctuations de Température et d'Humidité dans la Couche de Mélange Convective', *J. de Recherches Atmosphériques* **17**, 185–197.

Willis, G. E. and Deardorff, J. W.: 1974, 'A Laboratory Model of the Unstable Planetary Boundary Layer', *J. Atmos. Sci.* **31**, 1297–1307.

Wyngaard, J. C.: 1973, 'On Surface Layer Turbulence', in D. A. Haugen (ed.), *Workshop on Micrometeorology*, Amer. Meteor. Soc., Boston, Mass., USA, 101–149.

Wyngaard, J. C., Coté, O. R., and Izumi, Y.: 1971, 'Local Free Convection, Similarity, and the Budgets of Shear Stress and Heat Flux', *J. Atmos. Sci.* **28**, 1171–1182.

Wyngaard, J. C., Pennell, W. T., Lenschow, D. H., and LeMonde, M. A.: 1978, 'The Temperature-humidity Covariance Budget in the Convective Boundary Layer', *J. Atmos. Sci.* **35**, 47–58.